Computational modelling of 1D blood flow with variable mechanical properties and its application to the simulation of wave propagation in the human arterial system

S. J. Sherwin[1,*,†], L. Formaggia[2], J. Peiró[1] and V. Franke[1]

[1]*Biomedical Flow Group, Department of Aeronautics, Imperial College London, South Kensington Campus, London SW7 2AZ, U.K.*

[2]*Département de Mathématiques, EPFL, Lausanne, Switzerland. Current address: MOX, Modelling and Scientific Computing, Dipartamento di Matematica "F. Brioschi", Politecnico di Milano, Piazza L. da Vinci, 20133 Milano, Italy*

SUMMARY

In this paper we numerically investigate a one-dimensional model of blood flow in human arteries using both a discontinuous Galerkin and a Taylor–Galerkin formulation. The derivation of the model and the numerical schemes are detailed and applied to two model numerical experiments. We first study the effect of an intervention, such the implantation of a vascular prosthesis (e.g. a stent), which leads to an abrupt variation of the mechanical characteristics of an artery. We then discuss the simulation of the propagation of pressure and velocity waveforms in the human arterial tree using a simplified model consisting of the 55 main arteries. Copyright © 2003 John Wiley & Sons, Ltd.

KEY WORDS: 1D blood flow; computational haemodynamics; discontinuous Galerkin methods; Taylor–Galerkin methods; fluid–structure interaction

1. INTRODUCTION

The growing interest in the mathematical and numerical   modelling of biomedical systems and, in particular, the human cardiovascular system, is supported by the numerous works which have appeared on the subject in recent years, for example [1–4] and the references therein. Within this context, the application of simplified models have been shown to provide

---

* Correspondence to: S. J. Sherwin, Biomedical Flow Group, Department of Aeronautics, Imperial College London, South Kensington Campus, London, SW7 2 AZ, U.K.
† E-mail: s.sherwin@imperial.ac.uk

useful information for the practitioners at a reasonable computational cost [5] and this suggests that such models could provide a suitable tool for patient-specific medical planning of interventions.

In this paper we focus on the application of a one-dimensional model of blood flow in compliant vessels to study the effect of local narrowing or stiffening of an artery on the flow and wave propagation patterns. Such a situation can occur due to a stent implantation or the presence of a vascular prosthesis. A common pathology in the human circulatory system is the onset of atherosclerotic plaques that cause a restriction of the arterial lumen called a stenosis. In the most severe cases this may hinder, or even stop, the flow of blood. One of the present techniques to treat this problem is the implantation of a *stent* (an expandable metal mesh) into the affected region which has the purpose of returning the artery lumen to approximately its original shape. Whenever possible, this procedure is preferred to more invasive ones, such as surgical by-pass.

Nevertheless, besides other effects, the presence of a stent causes an abrupt variation in the elastic properties of the vessel wall, since the stent is usually far more rigid than the soft arterial tissue. This may cause a disturbance in the blood flow pattern and wall displacement with the appearance of reflected waves. Indeed, the so-called pressure pulse generated by the interaction between the blood flow and the compliance of the circulatory system is intrinsically related to the elastic properties of the arteries. The alteration in the pressure pattern is even more significant in the case of vascular prosthesis in the large arteries, for example, where stents are used to treat aortic or femoral aneurisms. The superposition of the waves reflected by the prosthesis or the stent with the pressure pulse produced by the heart can generate localised pressure peaks. Should these peaks occur at a suture line, the failure of an aortic or femoral prosthesis could be catastrophic.

Wave reflection also occurs at the branching of the arteries in the vascular system and this should be accounted for in considering the effect in pressure and waveforms at a given artery due to changes in cardiac output, geometry and elastic properties elsewhere in the arterial tree. The one-dimensional model of the compliant vessel can be adapted for the simulation of wave propagation in the arterial tree by imposing suitable interface conditions at the branching points.

In this paper we build upon the work of Formaggia *et al.* [6] and detail the construction of two numerical discretisations of the one-dimensional equations with abrupt changes in material properties. Section 2 outlines the governing equations and Section 3 analyses the characteristic system for the hyperbolic system of equations and provides a framework to discuss the appropriate specification of boundary conditions. We discuss the discretization of the hyperbolic system using the discontinuous Galerkin method in Section 4 and using a Taylor–Galerkin approach in Section 5. Finally Section 7 presents numerical results for vessels with variable material properties and a simulation of wave propagation in a model of the arterial system composed by the main 55 arteries.

2. GOVERNING EQUATIONS

We consider a simple compliant tube, illustrated in Figure 1, as a model of the artery. Following Brook *et al.* [7] we write the system of equations representing continuity of mass
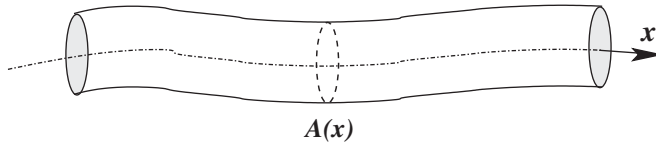
Figure 1. Simple compliant tube.

and momentum, for $a \leqslant x \leqslant b$ and $t > 0$, as

$$\frac{\partial A}{\partial t} + \frac{\partial Q}{\partial x} = 0$$

$$\frac{\partial Q}{\partial t} + \frac{\partial}{\partial x}\left(\alpha \frac{Q^2}{A}\right) + \frac{A}{\rho}\frac{\partial p}{\partial x} + K_R \frac{Q}{A} = 0 \tag{1}$$

where the x is the axial direction, $A = A(x,t) = \int_S d\sigma$ is the area of a cross section S, $Q = Q(x,t)$ is the mass flux across a section, ρ is the density of the blood which is taken to be constant, p is the internal pressure and $u(x,t) = Q(x,t)/A(x,t)$ denotes the velocity of the fluid averaged across the section. The term α is the momentum-flux correction coefficient, defined as

$$\alpha(x,t) = \frac{\int_S u^2 \, d\sigma}{Au^2}$$

In the following we will assume $\alpha = 1$ which is equivalent to assuming a flat velocity profile. Even though this might seem a crude assumption since the velocity profile of blood in any section S does indeed vary in time,[‡] comparison with experimental data [8] has shown that blood velocity profiles are rather flat on average and, furthermore, this assumption simplifies the analysis. However, we should stress that the methods to be presented in the following sections may be readily extended to the case of $\alpha \neq 1$. The term K_R is a strictly positive quantity which represents the viscous resistance of the flow per unit length of tube. The unknowns in this system are p, A and Q. Their number exceeds the number of equations and a common way to close the system is to explicitly provide an algebraic relationship between the pressure of the vessel p and the vessel area A. For example, by assuming *static equilibrium* in the radial direction of a cylindrical tube, one can derive a pressure relationship of the form

$$p = p_{\text{ext}} + \beta(\sqrt{A} - \sqrt{A_0}) \tag{2}$$

where

$$\beta = \frac{\sqrt{\pi}h_0 E}{(1-v^2)A_0}$$

Here h_0 and $A_0 = A_0(x)$ denote the vessel thickness and sectional area, respectively, at the equilibrium state $(p,Q) = (p_{\text{ext}}, 0)$, $E = E(x)$ is the Young modulus, p_{ext} is the external pres-

---

[‡]The analytical solution of pulsatile flow in a straight cylindrical elastic tube is given in Reference [9]. Analytical solutions for an initially stressed, anisotropic elastic tube are presented in Reference [10].

sure, assumed constant, and v is the Poisson ratio. This ratio is typically taken to be $v = 1/2$ since biological tissue is practically incompressible.

The system of equations (1) can be expressed alternatively in terms of the variables (A, u). By simple manipulations one gets

$$\frac{\partial A}{\partial t} + \frac{\partial Au}{\partial x} = 0$$

$$\frac{\partial u}{\partial t} + u\,\frac{\partial u}{\partial x} + \frac{1}{\rho}\,\frac{\partial p}{\partial x} + K_{\mathrm{R}} u = 0 \tag{3}$$

Both systems (1) and (3) may be written in conservation form. For the system (A, Q) we will write

$$\frac{\partial \mathbf{Q}}{\partial t} + \frac{\partial \mathbf{G}}{\partial x}(\mathbf{Q}) = \mathbf{B}(\mathbf{Q}) \tag{4}$$

with

$$\mathbf{Q} = \begin{bmatrix} A \\ Q \end{bmatrix}, \quad \mathbf{G} = \begin{bmatrix} Q \\ \frac{Q^2}{A} + \frac{\beta}{3\rho} A^{3/2} \end{bmatrix} \quad \text{and} \quad \mathbf{B} = \begin{bmatrix} 0 \\ -K_{\mathrm{R}}\frac{Q}{A} + \frac{A}{\rho}\frac{\mathrm{d}\beta}{\mathrm{d}x}(A_0^{1/2} - \frac{2A^{1/2}}{3}) \end{bmatrix} \tag{5}$$

For the (A, u) system we have

$$\frac{\partial \mathbf{U}}{\partial t} + \frac{\partial \mathbf{F}}{\partial x}(\mathbf{U}) = \mathbf{S}(\mathbf{U}) \tag{6}$$

with

$$\mathbf{U} = \begin{bmatrix} A \\ u \end{bmatrix}, \quad \mathbf{F} = \begin{bmatrix} Q \\ p_t \end{bmatrix} \quad \text{and} \quad \mathbf{S} = \begin{bmatrix} 0 \\ -K_{\mathrm{R}} u \end{bmatrix} \tag{7}$$

Here

$$p_t = \frac{u^2}{2} + \frac{p}{\rho} \tag{8}$$

denotes the *total pressure* (scaled by the constant density).

The two weak forms are equivalent for smooth solutions, in particular when A and Q are C^1 continuous functions with respect to both arguments and A is strictly positive. Otherwise, the proper conservation system is the one in the (A, Q) variables, since it derives directly from the basic physical principle of conservation of mass and momentum. Nevertheless, the solutions within each of the approaches presented in this paper will be sufficiently smooth to favour the use of the (A, u) system which has a simpler structure.

More precisely, the (A, u) system expressed by Equations (3) and the (A, Q) system expressed by Equations (1) will be starting points of the numerical schemes discussed in Sections 4 and 5, respectively. In using both systems we will assume the algebraic pressure-area relationship (2) in all that follows.

3. CHARACTERISTIC SYSTEM

3.1. Characteristic equations

Considering the pressure–area relationship (2) and assuming that $\beta = \beta(x)$ and $A_0 = A_0(x)$ we recall that applying the chain rule we obtain

$$\frac{\partial p}{\partial x} = \frac{\partial p}{\partial A}\frac{\partial A}{\partial x} + \frac{\partial p}{\partial \beta}\frac{\partial \beta}{\partial x} + \frac{\partial p}{\partial A_0}\frac{\partial A_0}{\partial x}$$

where

$$\frac{\mathrm{d}p}{\mathrm{d}A} = \frac{\beta}{2\sqrt{A}}$$

System (3) can therefore be written in quasi-linear form as

$$\frac{\partial \mathbf{U}}{\partial t} + \mathbf{H}\frac{\partial \mathbf{U}}{\partial x} = \begin{bmatrix} A \\ u \end{bmatrix}_t + \begin{bmatrix} u & A \\ c^2/A & u \end{bmatrix}\begin{bmatrix} A \\ u \end{bmatrix}_x = \begin{bmatrix} 0 \\ f \end{bmatrix} \tag{9}$$

where

$$c^2 = \frac{A}{\rho}\frac{\partial p}{\partial A} = \frac{\beta A^{1/2}}{2\rho} \quad \text{and} \quad f = \frac{1}{\rho}\left[K_\mathrm{R}u - \frac{\partial p}{\partial \beta}\frac{\partial \beta}{\partial x} + \frac{\partial p}{\partial A_0}\frac{\partial A_0}{\partial x}\right]$$

Under the assumption that $A > 0$, which is indeed a necessary condition to have a physically relevant solution, the matrix $\mathbf{H}$ has two real eigenvalues $\lambda_{1,2} = u \pm c$ and the corresponding left eigenmatrix $\mathbf{L}$ is

$$\mathbf{L} = \begin{bmatrix} \mathbf{l}_1^T \\ \mathbf{l}_2^T \end{bmatrix} = \begin{bmatrix} \frac{c}{A} & 1 \\ -\frac{c}{A} & 1 \end{bmatrix}$$

For the typical values of velocity, vessel area and elastic parameter β encountered in arteries under physiological conditions, we have that $\lambda_1 > 0$ and $\lambda_2 < 0$. Therefore our system is strictly hyperbolic and subcritical.

We recall some of the main results regarding the hyperbolic system at hand. It has been found in Reference [11] that, using a slightly different expression for the pressure–area relationship and under some reasonable conditions on the smoothness of boundary and initial data, the solution of system (1) remains smooth. Two critical assumptions to reach this conclusion are the pulsatility of the inflow data and a bound on the length of the tube; both are verified for physiological flow in the human arterial tree. In the same work it is shown that, if the solution is smooth and the initial and boundary data are such that $A > 0$, A remains strictly positive for all times. In Reference [12] an energy inequality was derived which bounds a measure of the energy of the hyperbolic system in terms of the initial and boundary data. Furthermore, in the same work it has been found that the quantity

$$s = \frac{1}{2}\rho A u^2 + \int_{A_0}^{A}(p - p_\mathrm{ext})\,\mathrm{d}A$$

is an entropy function for the system with associated flux equal to $F_s = Qp_t$.

The characteristic variables can be determined by integrating the differential system $\partial_U W = L$. It may be shown that this is possible for our problem and that the two characteristic variables are

$$W_1 = u + 4c = u + 4A^{1/4}\sqrt{\frac{\beta}{2\rho}} \tag{10}$$

$$W_2 = u - 4c = u - 4A^{1/4}\sqrt{\frac{\beta}{2\rho}} \tag{11}$$

Since $\beta > 0$, we may write, as previously reported in Reference [6], the variables (A, u) in terms of (W_1, W_2) as

$$A = \left[\frac{(W_1 - W_2)}{4}\right]^4 \left(\frac{\rho}{2\beta}\right)^2 \quad u = \frac{(W_1 + W_2)}{2} \tag{12}$$

In the case where $f = 0$, Equations (9) can be transformed in a decoupled system of equations for the characteristic variables, which component wise reads

$$\begin{aligned}
\frac{\partial W_1}{\partial t} + \lambda_1 \frac{\partial W_1}{\partial x} &= 0 \\
\frac{\partial W_2}{\partial t} + \lambda_2 \frac{\partial W_2}{\partial x} &= 0
\end{aligned} \tag{13}$$

3.2. Boundary conditions

The characteristic analysis and the fact that for physiological conditions the flow is subcritical (i.e. $\lambda_1 > 0$ and $\lambda_2 < 0$) leads us to the conclusion that only one boundary condition has to be imposed at each end of the tube. Different type of boundary conditions may be envisaged. Non-reflecting boundary conditions are those that allow the simple wave associated with the characteristics exiting the domain to leave without spurious reflections. Typically those conditions are expressed in terms of the characteristic variables. In References [13, 14] non-reflecting boundary conditions for an hyperbolic problem like (4) are provided as

$$\mathbf{l}_1 \left[\frac{\partial \mathbf{U}}{\partial t} - \mathbf{B(U)}\right]_{x=a} = 0, \qquad \mathbf{l}_2 \left[\frac{\partial \mathbf{U}}{\partial t} - \mathbf{B(U)}\right]_{x=b} = 0$$

For $\mathbf{B(U)} = \mathbf{0}$ they are equivalent to imposing a constant value for the entering characteristics, otherwise these relations account for the 'natural decay' due to the presence of the source term. With those conditions the amplitude of the incoming waves is constant in time (or may vary only because of the source term). In our case a condition of this type may be convenient at the outlet section (i.e. $x = b$), while at the inlet ($x = a$) we would like to prescribe some given values of pressure or flux data coming either from measurement or other models.

The hyperbolic system at hand allows us to impose either a flux Q (or velocity u) or area A at $x = a$. For instance we may impose

$$A(a, t) = g(t), \quad t > 0$$

where g is a known function obtained, for instance, from the knowledge of the pressure time variation at $x = a$. This type of condition is clearly of reflective type and the simple wave associated to the outgoing characteristic (W_2 in this case) may be partly reflected back into the computational domain. Yet, this reflection is a physical one.

It is also possible to have available values of both pressure (and thus area) and flux variations at the inlet. For instance, measurements of pressure pulse together with flux data could be obtained from Doppler ultrasound. Clearly the hyperbolic system does not allow to impose both conditions at the same time. However, it is known [15] that given a state $\mathbf{U}_0$ at a given time, one may construct a set of allowable boundary conditions which is given by the $\tilde{\mathbf{U}}$ which are obtained from $\mathbf{U}_0$ by the solution of a Riemann problem. This fact will be exploited in the implementation of the boundary conditions for one of the proposed numerical schemes that solves the Riemann problem in an approximate fashion.

In dealing with the numerical simulation of our hyperbolic system, the boundary conditions must be supplemented with additional conditions which allow us to obtain a complete set of values for $\mathbf{U}$ at the two boundaries. These are the so-called compatibility conditions which read

$$\mathbf{l}_2 \left[\frac{\partial \mathbf{U}}{\partial t} + \frac{\partial \mathbf{F}}{\partial x}(\mathbf{U}) - \mathbf{B}(\mathbf{U}) \right]_{x=a} = 0, \qquad \mathbf{l}_1 \left[\frac{\partial \mathbf{U}}{\partial t} + \frac{\partial \mathbf{F}}{\partial x}(\mathbf{U}) - \mathbf{B}(\mathbf{U}) \right]_{x=b} = 0$$

In the schemes here presented we have implemented the compatibility conditions only approximately. More details are found in Section 6.

4. DISCONTINUOUS GALERKIN METHOD

The wave propagation speeds in the large arteries are typically an order of magnitude higher than the average flow speeds. As mentioned previously, the characteristic system is inherently subcritical and does not produce shock under physiological conditions. Therefore the numerical challenge is to propagate waves for many periods without suffering from excessive dispersion and diffusion errors. If the solution remains smooth then high-order methods are particularly attractive due to the fast convergence of the phase and diffusion properties with order of the scheme [16].

The discontinuous Galerkin method is an attractive formulation for high-order discretisation of hyperbolic conservation laws. Following the work of Cockburn and Shu [17] and Lomtev, Quillen and Karniadakis [18] we proceed as follows.

Considering the one-dimensional hyperbolic system (3) in conservative form and assuming that $K_R = 0$ we have

$$\frac{\partial \mathbf{U}}{\partial t} + \frac{\partial \mathbf{F}}{\partial x} = 0 \tag{14}$$

where

$$\mathbf{U} = \begin{bmatrix} U_1 \\ U_2 \end{bmatrix} = \begin{bmatrix} A \\ u \end{bmatrix} \quad \mathbf{F} = \begin{bmatrix} F_1 \\ F_2 \end{bmatrix} = \begin{bmatrix} uA \\ \frac{u^2}{2} + \frac{p}{\rho} \end{bmatrix}$$

To solve this system in a domain $\Omega = (a, b)$ discretised into a mesh of N_{el} elemental non-overlapping regions $\Omega_e = (x_e^l, x_e^u)$, such that $x_e^u = x_{e+1}^l$ for $e = 1, \ldots, N_{\mathrm{el}}$, and

$$\bigcup_{e=1}^{N_{\mathrm{el}}} \bar{\Omega}_e = \bar{\Omega}$$

we start by constructing the weak form of (14), i.e.

$$\left(\frac{\partial \mathbf{U}}{\partial t}, \boldsymbol{\psi}\right)_\Omega + \left(\frac{\partial \mathbf{F}}{\partial x}, \boldsymbol{\psi}\right)_\Omega = 0 \tag{15}$$

where $\boldsymbol{\psi}$ represents an arbitrary function in Ω and

$$(\mathbf{u}, \mathbf{v})_\Omega = \int_\Omega \mathbf{u}\mathbf{v}\,\mathrm{d}x$$

is the standard $\mathbf{L}^2(\Omega)$ inner product. Decomposing the integral into elemental regions we obtain

$$\sum_{e=1}^{N_{\mathrm{el}}} \left[\left(\frac{\partial \mathbf{U}}{\partial t}, \boldsymbol{\psi}\right)_{\Omega_e} + \left(\frac{\partial \mathbf{F}}{\partial x}, \boldsymbol{\psi}\right)_{\Omega_e} \right] = 0 \tag{16}$$

Integrating the second term by parts leads to

$$\sum_{e=1}^{N_{\mathrm{el}}} \left\{ \left(\frac{\partial \mathbf{U}}{\partial t}, \boldsymbol{\psi}\right)_{\Omega_e} - \left(\mathbf{F}, \frac{\mathrm{d}\boldsymbol{\psi}}{\mathrm{d}x}\right)_{\Omega_e} + [\boldsymbol{\psi} \cdot \mathbf{F}]_{x_e^l}^{x_e^u} \right\} = 0 \tag{17}$$

To get the discrete form of our problem we choose $\mathbf{U}$ to be in the finite space of $\mathbf{L}^2(\Omega)$ functions which are polynomial of degree P on each element. We indicate an element of such space using the superscript δ. We also note that $\mathbf{U}^\delta$ may be discontinuous across inter-element boundaries. However to attain a global solution in the domain Ω we need to allow information to propagate between the elemental regions. Information is propagated between elements by upwinding the boundary flux, $\mathbf{F}$, in the third term of Equation (17). Denoting the upwinded flux as $\mathbf{F}^u$, the discrete weak formulation can now be written as

$$\sum_{e=1}^{N_{\mathrm{el}}} \left\{ \left(\frac{\partial \mathbf{U}^\delta}{\partial t}, \boldsymbol{\psi}^\delta\right)_{\Omega_e} - \left(\mathbf{F}(\mathbf{U}^\delta), \frac{\mathrm{d}\boldsymbol{\psi}^\delta}{\mathrm{d}x}\right)_{\Omega_e} + [\boldsymbol{\psi}^\delta \cdot \mathbf{F}^u]_{x_e^l}^{x_e^u} \right\} = 0 \tag{18}$$

Following the traditional Galerkin approach, we choose the test function $\boldsymbol{\psi}^\delta$ within each element to be in the same discrete space as the numerical solution $\mathbf{U}^\delta$. At this point if we defined our polynomial basis and choose an appropriate quadrature rule we would now have a semi-discrete scheme. However, from an implementation point of view, the calculation of the second term in Equation (18) can be inconvenient and consequently we choose to integrate this term by parts once more to obtain

$$\sum_{e=1}^{N_{\mathrm{el}}} \left\{ \left(\frac{\partial \mathbf{U}^\delta}{\partial t}, \boldsymbol{\psi}^\delta\right)_{\Omega_e} + \left(\frac{\partial \mathbf{F}(\mathbf{U}^\delta)}{\partial x}, \boldsymbol{\psi}^\delta\right)_{\Omega_e} + [\boldsymbol{\psi}^\delta \cdot \{\mathbf{F}^u - \mathbf{F}(\mathbf{U}^\delta)\}]_{x_e^l}^{x_e^u} \right\} = 0 \tag{19}$$

We note that the information between elements is transmitted by the third boundary term as the difference between the upwinded and the local fluxes, $[\boldsymbol{\psi}^\delta \cdot [\mathbf{F}^u - \mathbf{F}(\mathbf{U}^\delta)]]_{x_e^l}^{x_e^u}$. This method can

be considered as a penalty method with an automatic procedure for determining the penalty parameter.

Finally we select our expansion bases to be polynomials of order P and expand our solution on each element e in terms of Legendre polynomials $L_p(\xi)$, i.e.

$$\mathbf{U}^\delta|_{\Omega_e}(x_e(\xi), t) = \sum_{p=0}^{P} L_p(\xi) \hat{\mathbf{U}}_e^p(t)$$

where, following standard finite element techniques, we consider ξ in the reference element $\Omega_{st} = \{-1 \leqslant \xi \leqslant 1\}$ and introduce the elemental affine mapping

$$x_e(\xi) = x_e^l \frac{(1 - \xi)}{2} + x_e^u \frac{(1 + \xi)}{2}$$

We note that the choice of discontinuous discrete solution and test functions allow us to decouple the problem on each element, the only link coming through the upwinded boundary fluxes. Legendre polynomials are particularly convenient because the basis is orthogonal with respect to the $\mathbf{L}^2(\Omega_e)$ inner product and Equation (19) turns out to be equivalent to solving, componentwise, for all elements e

$$J_e \frac{\partial \hat{U}_{i,e}^p}{\partial t} = -J_e \left(\frac{\partial F_i}{\partial x}, L_p \right)_{\Omega_e} - [L_p [F_i^u - F_i(\mathbf{U}^\delta)]]_{x_e^l}^{x_e^u} = 0, \quad p = 1, \ldots, P, \ i = 1, 2 \qquad (20)$$

where J_e is the Jacobian of the elemental mapping, $J_e = \frac{1}{2}(x_e^u - x_e^l)$. To complete the discretization we require a time integration scheme. Here we have adopted an Adams–Bashforth scheme. The calculation of the upwind flux $\mathbf{F}^u$ is discussed in Section 3. This upwinding process can also be used to impose the characteristic boundary conditions through the flux at the ends of the global domain Ω.

5. TAYLOR–GALERKIN METHOD

In this section we describe the numerical discretisation of the (Q, A) system described by Equation (1) recast in the conservation form (6) given by

$$\frac{\partial \mathbf{Q}}{\partial t} + \frac{\partial \mathbf{G}}{\partial x} = \mathbf{B}$$

where once again we have taken $R_K = 0$ and the expressions for $\mathbf{Q}$, $\mathbf{G}$ and $\mathbf{B}$ are given in (5).

We proceed to discretize equation (6) by adopting a second-order Taylor–Galerkin scheme, which is the finite element counterpart of the well known Lax–Wendroff finite difference scheme.

The presence of a non-constant source term and the explicit dependence of the momentum flux $\mathbf{G}$ on the variable x through $\beta(x)$ makes the derivation of the scheme slightly more complex. In the rest of this paper we will use the abridged notation

$$\mathbf{G_Q} = \frac{\partial \mathbf{G}}{\partial \mathbf{Q}}, \quad \mathbf{B_Q} = \frac{\partial \mathbf{B}}{\partial \mathbf{Q}}$$

We follow the usual route to derive the Lax–Wendroff scheme, by writing

$$\frac{\partial \mathbf{Q}}{\partial t} = \mathbf{B} - \frac{\partial \mathbf{G}}{\partial x} \tag{21}$$

$$\frac{\partial^2 \mathbf{Q}}{\partial t^2} = \mathbf{B_Q}\frac{\partial \mathbf{Q}}{\partial t} - \frac{\partial^2 \mathbf{G}}{\partial t \partial x} = \mathbf{B_Q}\frac{\partial \mathbf{Q}}{\partial t} - \frac{\partial}{\partial x}\left(\mathbf{G_Q}\frac{\partial \mathbf{Q}}{\partial t}\right)$$

$$= \mathbf{B_Q}\left(\mathbf{B} - \frac{\partial \mathbf{G}}{\partial x}\right) - \frac{\partial(\mathbf{G_Q B})}{\partial x} + \frac{\partial}{\partial x}\left(\mathbf{G_Q}\frac{\partial \mathbf{G}}{\partial x}\right) \tag{22}$$

We stress that, in contrast to the normal derivation of a Lax–Wendroff scheme, we have not further developed the x derivative of the fluxes, since for our problem

$$\frac{\partial \mathbf{G}}{\partial x} \neq \mathbf{G_Q}\frac{\partial \mathbf{Q}}{\partial x}$$

because of the dependence of $\mathbf{G}$ on x through β.

For the time discretisation, we consider a timestep Δt and indicate by a superscript n quantities computed at time $t^n = n\Delta t$. Applying, as in a standard Lax–Wendroff procedure, a truncated Taylor expansion in time around t^n and exploiting (21) and (22) we finally obtain the following time-marching scheme

$$\mathbf{Q}^{n+1} = \mathbf{Q}^n - \Delta t\frac{\partial}{\partial x}\left[\mathbf{G}^n + \frac{\Delta t}{2}\,\mathbf{G_Q^n B}^n\right]$$

$$- \frac{\Delta t^2}{2}\left[\mathbf{B_Q^n}\frac{\partial \mathbf{G}^n}{\partial x} - \frac{\partial}{\partial x}\left(\mathbf{G_Q^n}\frac{\partial \mathbf{G}^n}{\partial x}\right)\right] + \Delta t\left(\mathbf{B}^n + \frac{\Delta t}{2}\,\mathbf{B_Q^n B}^n\right) \tag{23}$$

Space discretization is carried out by using linear finite elements. To that purpose, let us subdivide the domain Ω into N_{el} finite elements Ω_e, of constant size h. We indicate by $\mathbf{V}_h$ the space of continuous vector functions defined on Ω, linear on each element, and with $\mathbf{V}_h^0$ the set formed by functions of $\mathbf{V}_h$ which are zero at $x = a$ and b. Furthermore, we omit the subscript Ω in the $\mathbf{L}^2(\Omega)$ vector product.

Using the notation

$$\mathbf{G}_{\text{LW}} = \mathbf{G} + (\Delta t/2)\mathbf{G_Q B}$$

$$\mathbf{B}_{\text{LW}} = \mathbf{B} + (\Delta t/2)\mathbf{B_Q B}$$

the finite element formulation of (23) is: for $n \geqslant 0$, find $\mathbf{Q}_h^{n+1} \in \mathbf{V}_h$ which satisfies

$$(\mathbf{Q}_h^{n+1}, \boldsymbol{\psi}_h) = (\mathbf{Q}_h^n, \boldsymbol{\psi}_h) + \Delta t\left(\mathbf{G}_{\text{LW}}^n, \frac{\partial \boldsymbol{\psi}_h}{\partial x}\right) - \frac{\Delta t^2}{2}\left(\mathbf{B_Q^n}\frac{\partial \mathbf{G}^n}{\partial x}\boldsymbol{\psi}_h\right)$$

$$- \frac{\Delta t^2}{2}\left(\mathbf{G_Q^n}\frac{\partial \mathbf{G}^n}{\partial x}, \frac{\partial \boldsymbol{\psi}_h}{\partial x}\right) + \Delta t(\mathbf{B}_{\text{LW}}^n, \boldsymbol{\psi}_h), \quad \forall \boldsymbol{\psi}_h \in \mathbf{V}_h^0 \tag{24}$$

The boundary values of $\mathbf{Q}_h^{n+1}$ are calculated using the technique described in Section 6.5. $\mathbf{Q}_h^0$ will also be taken as the finite element interpolant of the given initial data $\mathbf{Q}_0$.

In (24) we need to numerically integrate the terms containing the fluxes and sources. For the terms involving $\mathbf{G}^n$ and $\mathbf{G}_\mathbf{Q}^n$ we have projected each component on the finite element function space V_h via interpolation. The same applies for the other vector products which involve only $\mathbf{G}^n$ and $\mathbf{G}_\mathbf{Q}^n$.

As for the terms containing $\mathbf{B}^n$ and $\mathbf{B}_\mathbf{Q}^n$, we have adopted a slightly different approach in order to assure the strong consistency of the numerical scheme with respect to constant solutions. More precisely, we wanted to ensure that our numerical scheme exactly represented constant solutions of the differential problem. In view of this, the term $d\beta/dx$ has to be approximated by piecewise constants. Therefore, on each element (x_e^l, x_e^u) we have approximated $d\beta/dx$ by $[\beta(x_i^u) - \beta(x_i^l)]/h$. For the remaining terms we have applied the same technique adopted for the fluxes. This gives rise to a piecewise linear discontinuous representation for the source terms.

6. NUMERICAL BOUNDARY CONDITIONS

The numerical schemes (20) and (24) need to be complemented with boundary data $\mathbf{Q}$ or $\mathbf{U}$ at the boundaries of the domain Ω. We note that knowledge of W_1 and W_2 at the boundaries would in principle enable us to compute the corresponding values of $\mathbf{Q}$ or $\mathbf{U}$, thanks to relation (12). However, given that the propagation speed is subcritical, only one condition has to be assigned at each end for the well-posedness of the differential problem. The implementation of boundary conditions for the discontinuous Galerkin and Taylor–Galerkin schemes is discussed in the following sections.

6.1. Discontinuous Galerkin method: Flux upwinding

The boundary conditions in the discontinuous Galerkin method are imposed in an identical fashion to the flux upwinding term applied at the inter-elemental boundaries and therefore are discussed together in this section.

Here we will assume the problem remains subcritical, i.e. $c > u$, and therefore $\lambda_1 > 0$ and $\lambda_2 < 0$. We consider a point $x = x_e^u = x_{e+1}^l$ at the interface between elements e and $e+1$. Given a function f continuous on each element e and $e+1$, yet possibly discontinuous at x, we indicate by f_l and f_r its left and right limiting values, respectively. Equivalently,

$$f_l = f|_{\Omega_e}(x_e^u), \quad f_r = f|_{\Omega_{e+1}}(x_{e+1}^l)$$

The appropriate characteristic information at point x is given by

$$W_1 = u_l + 4A_l^{1/4}\sqrt{\frac{\beta_l}{2\rho}} \tag{25}$$

$$W_2 = u_r - 4A_r^{1/4}\sqrt{\frac{\beta_r}{2\rho}} \tag{26}$$
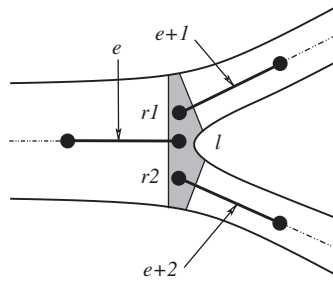
Figure 2. Arterial tree bifurcation: notation.

When β is continuous ($\beta_l = \beta_r$), $\mathbf{F}^u$ at point x is computed by posing $\mathbf{F}^u = \mathbf{F}(\mathbf{U}^u)$, where $\mathbf{U}^u = [A^u, u^u]^{\mathrm{T}}$ is computed from W_1 and W_2 given by Equations (25), (26) and applying Equations (12), i.e

$$\mathbf{F}(\mathbf{U}^u) = \begin{bmatrix} F_1(\mathbf{U}^u) \\ F_2(\mathbf{U}^u) \end{bmatrix} = \begin{bmatrix} A^u u^u \\ \frac{(u^u)^2}{2} + \frac{p(A^u)}{\rho} \end{bmatrix}$$

This upwinding is applied at all elemental interfaces, including the inflow and outflow, where W_1 (inflow) or W_2 (outflow) are now provided by the boundary conditions.

6.2. Discontinuous Galerkin method: Discontinuous material properties

For the case where the material properties are discontinuous across the interface then equations (25) need to be supplemented with additional information. A reasonable choice is to assume continuity of fluxes and thus impose that continuity of mass flux and total pressure across the interface, i.e.

$$Q = u_l A_l = u_r A_r \tag{27}$$

$$P_r = \rho \frac{u_l^2}{2} + \beta_l(\sqrt{A_l} - \sqrt{A_{l_0}}) = \rho \frac{u_r^2}{2} + \beta_r(\sqrt{A_r} - \sqrt{A_{r_0}}) \tag{28}$$

This interface conditions will preserve the conservation properties of (A, u) system. This approach would also permit a discontinuity of the vessel reference area A_0. Equations (25)–(28) are then solved in an iterative fashion to determine the values of u_l, u_r, A_l and A_r.

6.3. Discontinuous Galerkin method: Treatment of bifurcations

The 1D model of the compliant tube can be extended to handle the arterial tree by imposing suitable interface conditions at the bifurcations or branching points of the tree.

   In the presence of a bifurcation at the inter-elemental boundaries we consider, following the notation of Figure 2, a point $x = x_e^u = x_{e+1}^l = x_{e+2}^l$ at the interface between three elements e, $e+1$ and $e+2$. Similarly to the interface between two elements, a function f is continuous

on each element e, $e+1$ and $e+2$ and may be discontinuous at x, where f_l, f_{r1} and f_{r2} are the left and right limiting values

$$f_l = f|_{\Omega_e}(x_e^u), \quad f_{r1} = f|_{\Omega_{e+1}}(x_{e+1}^l), \quad f_{r2} = f|_{\Omega_{e+2}}(x_{e+2}^l)$$

At the bifurcation we have six unknowns: (A_l, u_l) in the parent vessel (left vessel in Figure 2), (A_{r1}, u_{r1}) in the upper daughter vessel, and (A_{r2}, u_{r2}) in the lower daughter vessel.

The first three equations required to solve the problem are obtained by imposing that the characteristic variables at point x in each vessel should remain constant. Their values are

$$W_1 = u_l + 4A_l^{1/4}\sqrt{\frac{\beta_l}{2\rho}} \tag{29}$$

$$W_{21} = u_{r1} - 4A_{r1}^{1/4}\sqrt{\frac{\beta_{r1}}{2\rho}} \tag{30}$$

$$W_{22} = u_{r2} - 4A_{r2}^{1/4}\sqrt{\frac{\beta_{r2}}{2\rho}} \tag{31}$$

At a bifurcation it is likely that β will be discontinuous. The other three equations required to close the problem are obtained from the continuity of mass flux and total pressure across the boundary of the elements at the bifurcation, i.e.

$$Q = u_l A_l = u_{r1} A_{r1} + u_{r2} A_{r2} \tag{32}$$

$$P_r = \rho\frac{u_l^2}{2} + \beta_l(\sqrt{A_l} - \sqrt{A_{l_0}}) = \rho\frac{u_{r1}^2}{2} + \beta_{r1}(\sqrt{A_{r1}} - \sqrt{A_{r1_0}}) \tag{33}$$

$$P_r = \rho\frac{u_l^2}{2} + \beta_l(\sqrt{A_l} - \sqrt{A_{l_0}}) = \rho\frac{u_{r2}^2}{2} + \beta_{r2}(\sqrt{A_{r2}} - \sqrt{A_{r2_0}}) \tag{34}$$

The six equations given by (29)–(34) define a non-linear system of algebraic equations which determine the values of (A_l, u_l), (A_{r1}, u_{r1}) and (A_{r2}, u_{r2}) at the bifurcation. These values are then used to evaluate the upwind flux at the elemental interfaces in the numerical discretization.

6.4. Discontinuous Galerkin method: Terminal vessels

The human arterial system is a network of large arteries branching out into many smaller arteries, arterioles and capillaries. We are usually interested in the results in the larger arteries in the network. Blood vessels further down the arterial tree maybe very small and numerous. To reduce the problem size only a small part of the network will be modelled. The networks of blood vessels further down the arterial system will also be transmitting backward travelling waves in the body, therefore at the boundary of the modelled arteries an approximation needs to be included for these reflections.

To model the reflected waves a reflection coefficient is applied to the waves exiting the terminal vessels. The reflection coefficient, R_t, is defined in Reference [19] as the ratio of the

magnitude of change of pressure across the reflected wave, dP, to the magnitude of change of pressure in the incident wave, ΔP. It is a function of the terminal resistance at the vessel outflow and is given by

$$R_t = \frac{dP}{\Delta P} = \frac{R_P - \rho c}{R_P + \rho c}$$

where R_P represents the resistance in the arterial network beyond the terminal vessel. The assumption adopted here for calculating the terminal resistance is that of Reference [20] who assumed that $R_P = P/U$ where P is the pressure upstream of the vessel and U is the mean velocity. The mean velocity was based on an even distribution of blood flow around the body and the venous pressure is assumed to be zero.

The value of R_t permits the outflow at the boundary to vary between a free outflow when $R_t = 0$ and a blockage when $R_t = 1$. Using this relationship and Equation (12) which relates the velocity u and the characteristic variables, W_1 and W_2, the velocity, $u^\star$, at the boundary can be specified to be

$$u^\star = \left[\frac{(u_0 + u_l)}{2} + 2(c_l - c_0) \right] (1 - R_t) \tag{35}$$

where u_0 and c_0 are the undisturbed states on the right-hand side at $t = 0$. The characteristic variable W_1 remains unaltered at the outflow boundary and is given as

$$W_1 = u_l + 4c_l = u^\star + 4c^\star$$

and therefore $c^\star$ at the boundary must be

$$c^\star = \left[\frac{u_l - u^\star}{4} \right] + c_l \tag{36}$$

We define the incoming wave, W_2, as

$$W_2 = u_r - 4c_r = u^\star - 4c^\star \tag{37}$$

Substituting Equations (35) and (36) into Equation (37) and choosing $c_l = c_r$ at the boundary, leads us to the values of u_r and A_r to be prescribed at the boundary, these are

$$u_r = (1 - R_t)[(u_0 + u_l) + 4(c_l - c_0)] - u_l$$

$$A_r = A_l$$

The characteristic variable, W_2, at the outflow can now be calculated using Equation (26).

6.5. Taylor–Galerkin method: Extrapolating characteristics

For the Taylor–Galerkin method we require information about the conservative variables at the ends of the domain, i.e. $\mathbf{Q}(a, t)$ and $\mathbf{Q}(b, t)$. To extract this from the characteristic information $W_1(a, t)$ and $W_2(b, t)$ we require an additional expression for the other characteristic variables $W_2(a, t)$ and $W_1(b, t)$ to recover $\mathbf{Q}$ using Equation (12) which must also be compatible with the original differential problem. In the current approach, we have adopted a technique based
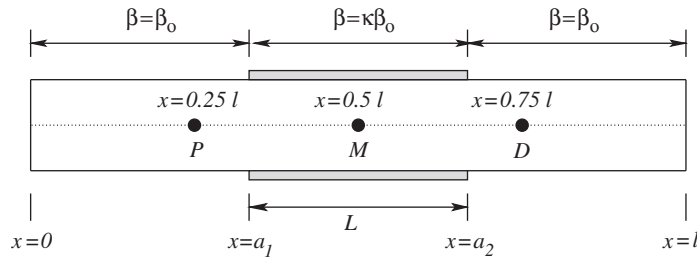
Figure 3. Test case layout.

on the extrapolation of the outgoing characteristics. We make the initial assumption that, at the boundary points $x = a$ and $x = b$, $d\beta/dx = 0$ and that K_R is small or zero. We then assume that in the vicinity of the boundary the flow is essentially governed by the characteristic system (13). An equivalent derivation for the (A, Q) system can be found in Reference [6]. Let us consider now the proximal boundary $x = a$ over a generic timestep (the distal boundary is treated in a similar fashion). We assume that $\mathbf{Q}^n$ is known and we linearise λ_2 in the second equation in (13) by taking its value at time t^n and at $x = a$. The solution corresponding to this linearised problem at the time level t^{n+1} gives

$$W_2^{n+1}(a) = W_2^n(-\lambda_2^n(a)\Delta t)$$

which is, in fact, a first-order extrapolation of the outgoing characteristic variable W_2 from the previous time level. Higher order extrapolations can also be applied. By using this information together with the value of W_1 provided by the boundary condition, $W_1^{n+1}(a, t)$, we are able to compute, using (12), the required boundary data, $\mathbf{Q}^{n+1}(0)$.

This technique may be extended to boundary conditions that are not given in terms of the characteristic variables. For instance, if a given law for the pressure $p(a, t) = \psi(t)$ is imposed at the proximal boundary.

7. RESULTS

In order to compare the results of the two numerical techniques we consider an example taken from Reference [6]. We consider a vessel of constant unit diameter and $l = 15$ units long as shown in Figure 3.

The material properties varies from a value of β_0 either side of an internal region $a_1 \leqslant x \leqslant a_2$ where it is increased to $\kappa\beta_0$. Using the data provided in Reference [6] we obtain that $\beta_0 = 451\,352$ and apply a density of $\rho = 1$ and $\kappa = 100$. This region of increased stiffness is chosen to be of length $L = 5$ units with $a_1 = 5$, and $a_2 = 10$. Finally the material properties along the length of the pipe are approximated using a C^1 continuous piecewise polynomial function over a width 2δ as indicated in Figure 4. In our problem δ was taken to be 0.5. Finally we consider the flow in the pipe to be initially at rest and impose an inflow pressure wave above the steady equilibrium in the form a solitary half sine wave as shown in Figure 5. This is represented by
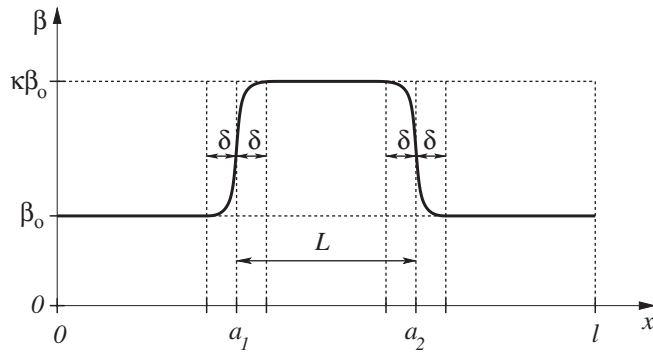
$$p(0, t) = 2000 \sin(2\pi t/T)H(T/2 - t)$$

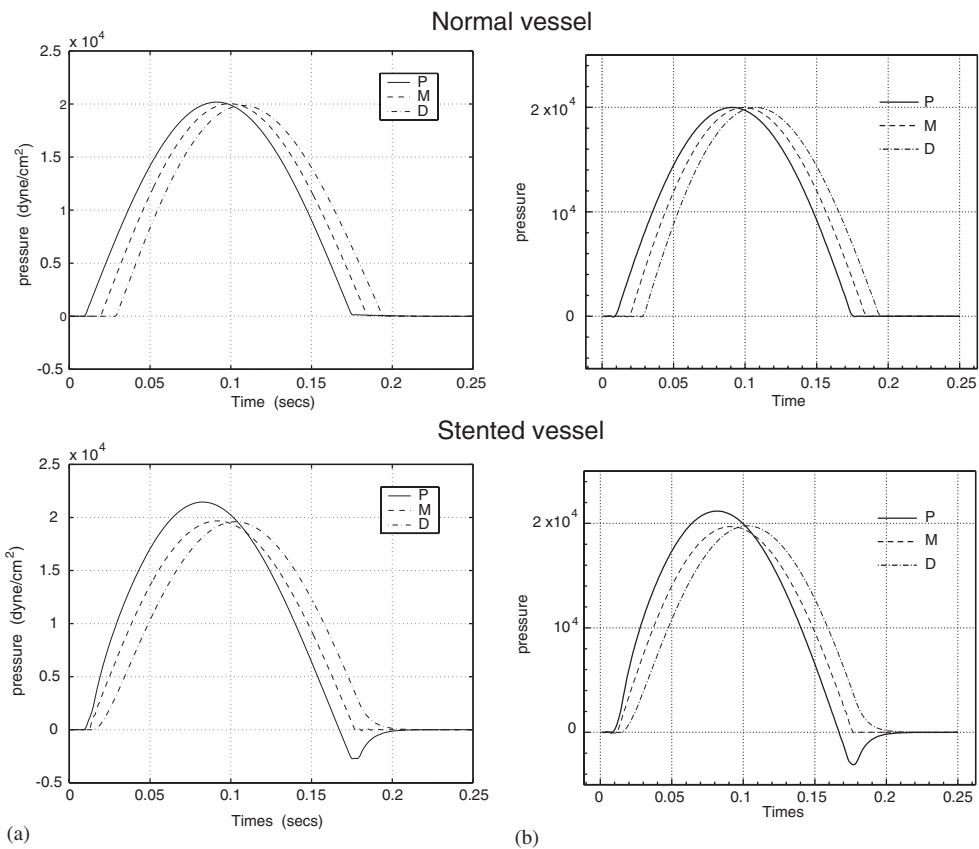Figure 4. Variation of wall properties in test case.

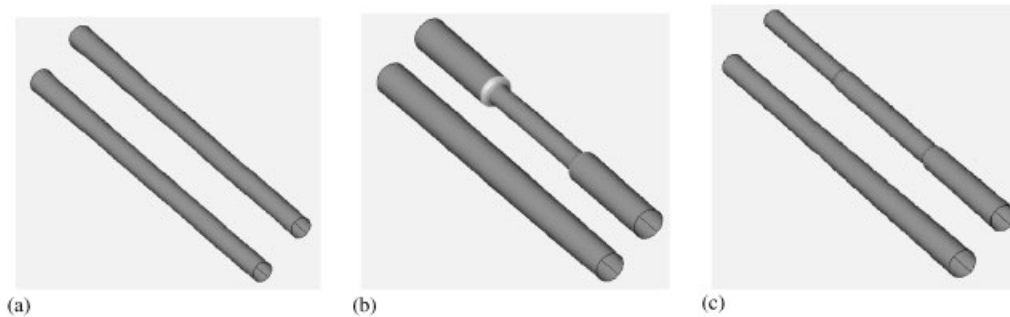Figure 5. Time history: (a) Taylor–Galerkin and (b) discontinuous Galerkin schemes.

Figure 6. Three dimensional interpretation of waves in stented (top) and normal vessel (bottom) (a) $t = 0.01$, (b) $t = 0.075$ and (c) $t = 0.175$. The displacement from A_0 has been magnified by a factor of 10.

with $T = 0.33$. $H(t)$ is the Heaviside step function which is defined as

$$H(t - a) = \begin{cases} 1 & t > a \\ 0 & t < a \end{cases}$$

Figure 5 shows a time history comparison between the Taylor–Galerkin (Figure 5(a)) and the discontinuous Galerkin (Figure 5(b)) schemes. The Taylor–Galerkin scheme uses 105 non-uniform element refined about a_1 and a_2 whilst the discontinuous Galerkin method uses 5 elements of polynomial order $P = 6$. One element is employed to represent both material transition regions and three more elements are placed in the regions of constant properties. A timestep of $\Delta t = 2 \times 10^{-6}$ was adopted in all computations. In Figure 5 we see the time history over a time period 0.25 at three points: distal (D), medial (M) and proximal (P) to the stented region as indicated in Figure 3.

In the top of these figures we considered the case without variation in material properties, i.e. $\kappa = 1$. In this case we see that the pressure wave propagates to the right at a constant speed. However when we introduce the material variation as shown in the bottom plots there is an increase in the peak of the proximal waveform due to a reflection of the incoming waves at the region of increased stiffness. Reasonable agreement is found between these two different numerical implementations. A representation of the wave propagation in the stented and non-stented vessels at $t = 0.01, 0.075$ and 0.175 is shown in Figure 6. The displacement of the cross-sectional area variation from the mean value A_0 had been magnified by a factor of 10 in these figures.

As a further test case for the discontinuous Galerkin method we consider a normalised pipe of unit area, $A_0 = 1$ and normalise the mean velocity so that it has a unit value too. Physiologically we expect the wave speed to be an order of magnitude higher than the mean velocity and so we prescribe a mean speed of sound $c_0 = \sqrt{\beta/(2\rho)}A_0^{1/4} = 10$. This can be achieved by selecting $\beta = 10$ and $\rho = 0.5$.

At many arterial locations there is a strong velocity acceleration due to the systolic motion of the heart followed by a deceleration associated with diastolic motion. Although the flow waveform from the aortic valve might be modelled as a half-sine wave the reflections due
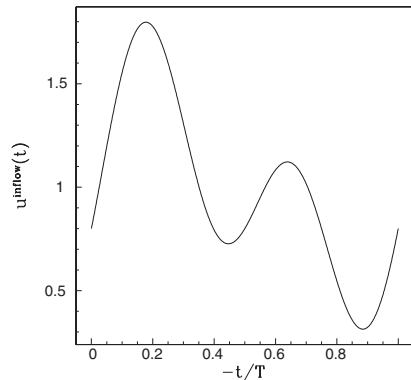
Figure 7. Inflow velocity boundary conditions.

to bifurcations in the arterial tree cause the local flow waveforms to differ considerably from this input [21]. We therefore take an input flow waveform, shown in Figure 7, of the form

$$u^{\text{inflow}}(t) = 1 - 0.4\sin(wt) - 0.4\sin(2wt) - 0.2\cos(2wt)$$

where $w = 2\pi/T$ and T is the time period. Making the assumption that the spatial wavelength λ is approximately 100 times larger than the vessel diameter, we choose $T = 10$ since for the linear case $\lambda = c_0 T \approx 100$.

Since we are considering a problem with a wavelength of $\lambda = 100$, in order to observe the wave as a function of the artery centreline we will consider a computational interval $(-100, 100)$. The domain is subdivided into $N_{\text{el}} = 10$ elements of equal length and a polynomial order of $P = 7$ is applied within each element. The solution at times $t = 2.5, 12.5$ and 20 is shown in Figure 8(a). After $t = 20$ the solution remains time periodic with a time period of $T = 10$. We note that the solution profiles for $u(x)$ and $A(x)$ are similar in shape. This is to be expected if we consider the characteristic variables, $W_1(x)$ and $W_2(x)$ at the same times. Figure 8(b) shows that the solution only contains a right travelling $W_1(x)$ wave and, furthermore, Equation (12) indicates that $u(x)$ and $A(x)$ are proportional to powers of $W_1(x)$.

In these simulations we have imposed the boundary conditions using the characteristic upwinding through the flux vector as discussed in Section 6.1. To apply this boundary condition, the conservative variables to the left of $x = -100$ were set to $u_l(-100, t) = u^{\text{inflow}}(t)$ and $A_l(-100, t) = 1$. The conservative variables to the right of $x = 100$ were set to $u_r(100, t) = 1$ and $A_r(100, t) = 1$. A second-order time stepping scheme was applied with a timestep of $\Delta t = 0.005$.

We note that the second period of the wave in Figure 8 is slightly steeper than the first due to the nonlinearity of the system. Also the curve has not quite achieved two periods in the domain since the right travelling wave is moving at a speed $u + c$ rather than u. In practice this domain is not physically realizable since if a large artery has an approximate diameter of 1 cm then the artery would have to be 2 m long! Clearly the wave would normally come interact with a arterial junction and undergo wave reflections before it is able to propagate so far. This is convenient since when we consider the above problem over a longer domain the non-linearity of the wave is sufficient for a shock to form where the peak of the wave catches up with its trough.
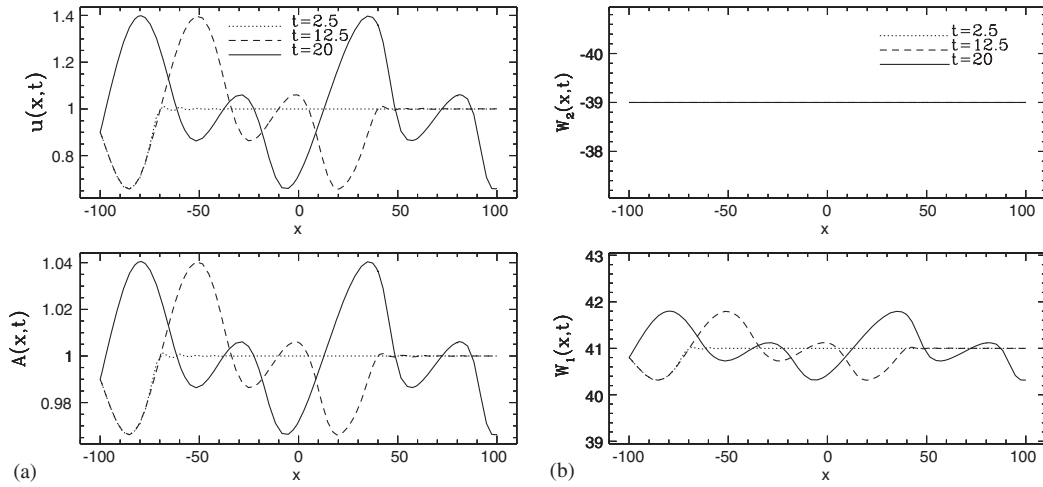
Figure 8. Advection of right travelling wave in continuous material at times $t = 2.5, 7.5$ and 20: (a) conservative variables and (b) characteristic variables.
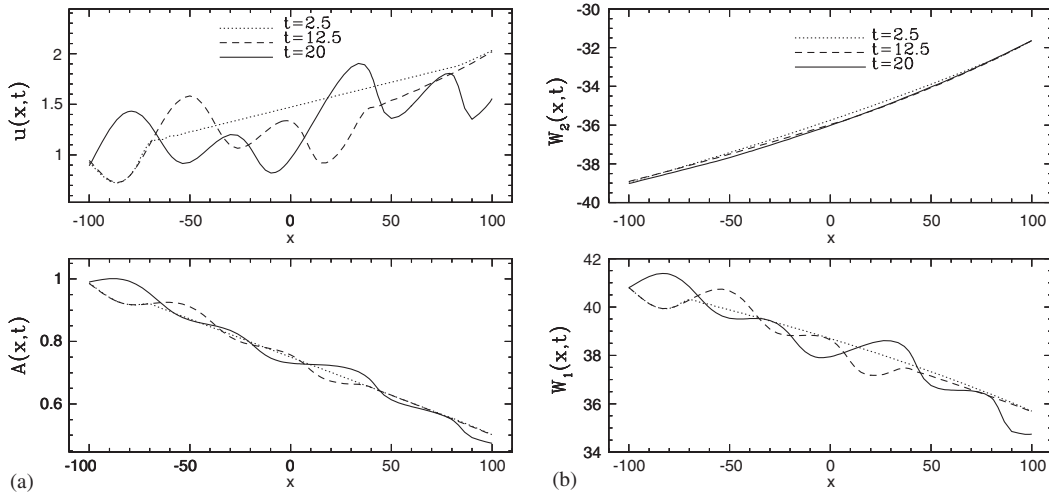

Figure 9. Advection of right travelling wave in tapered pipe at times $t = 2.5, 7.5$ and 20: (a) conservative variables and (b) characteristic variables.

As a final example we consider the previous case in a tapering pipe as shown in Figure 9. The pipe was prescribed to have an undeformed cross sectional area which linearly varies from $A(-100, t) = 1$ to $A(100, t) = 0.5$. As initial conditions we specified that the mass flux was constant and so u varied linearly from $u(-100, t) = 1$ to $u(100, t) = 2$. The same boundary conditions were also applied to the left-hand side. However the right-hand boundary conditions were modified to be compatible with the initial conditions, i.e. $A_r(100, t) = 0.5$ and $u_r(100, t) = 2$.
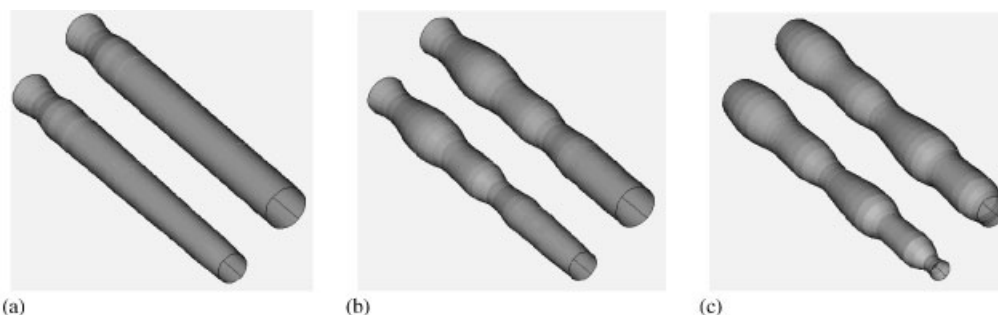
Figure 10. Three dimensional interpretation of waves in normal (top) and tapered (bottom) vessels (a) $t = 2.5$, (b) $t = 12.5$ and (c) $t = 20$. The displacement form $A_0(x)$ has been magnified by a factor of 10 and the x-axis is scaled by a factor of $1/20$.

In Figure 9 we once again show the conservative and characteristic variables at times $t = 2.5, 12.5$ and 20 similar to Figure 8. We note that for this example more than two periods are present in the $u(x, t)$ plot as compared to less than two periods in Figure 8. This is to be expected since the basic wave-speed, $c_0 = \sqrt{\beta/(2\rho)}A_0^{1/4}$, decreases along the pipe as the area decreases provided that we keep β constant, i.e. we assume that $h_0/\sqrt{A_0}$ is constant. In Figure 10 we show a three dimensional representation of the constant and tapered pipe at times $t = 2.5, 12.5$ and 20. Once again the displacement from $A_0(x)$ had been magnified by a factor or 10 and the x-axis has also been scaled by a factor of $1/20$.

7.1. Discontinuous Galerkin method: Arterial network

The human circulation is made up of a complex network of vessels: arteries and veins. Arteries are compliant vessels that carry the oxygenated blood to the different parts of the body. Their compliance accommodates the volumetric changes required to move blood, which is an incompressible fluid, through the vascular system. A simplified arterial network containing the 55 largest arteries in the human body was proposed and modelled using electrical circuits by Westerhof in Reference [22]. This reference provides physiological data for radii, wall thickness, length and elastic moduli for each of the 55 arteries. Terminal resistances for the model have been calculated in Reference [20] using the method described in Section 6.4. Wang and Parker [21] found that ill-matched forward travelling waves at the bifurcations would obscure the reflections from the terminal segments and adjusted the radii of the 55 arteries to give well-matched forward travelling waves, i.e. waves that give small reflections at the bifurcations. The bifurcations are not well-matched for backward travelling waves.

We have adopted the modifications proposed in Reference [21] to the published models [22, 20] to compute the pulsatile one-dimensional blood flow through the arterial system using the discontinuous Galerkin method. Figure 11 shows the connectivity of the arteries used in our model of the arterial network. The numerical values of the parameters of the arterial tree are included in Table I. The effect of adding terminal resistance is also considered.

The flow in the 55 arteries is assumed initially to be at rest. The density of blood was taken to be $\rho = 1.021 \times 10^3$ Kg/m^3. A periodic half sine wave is imposed as an input wave
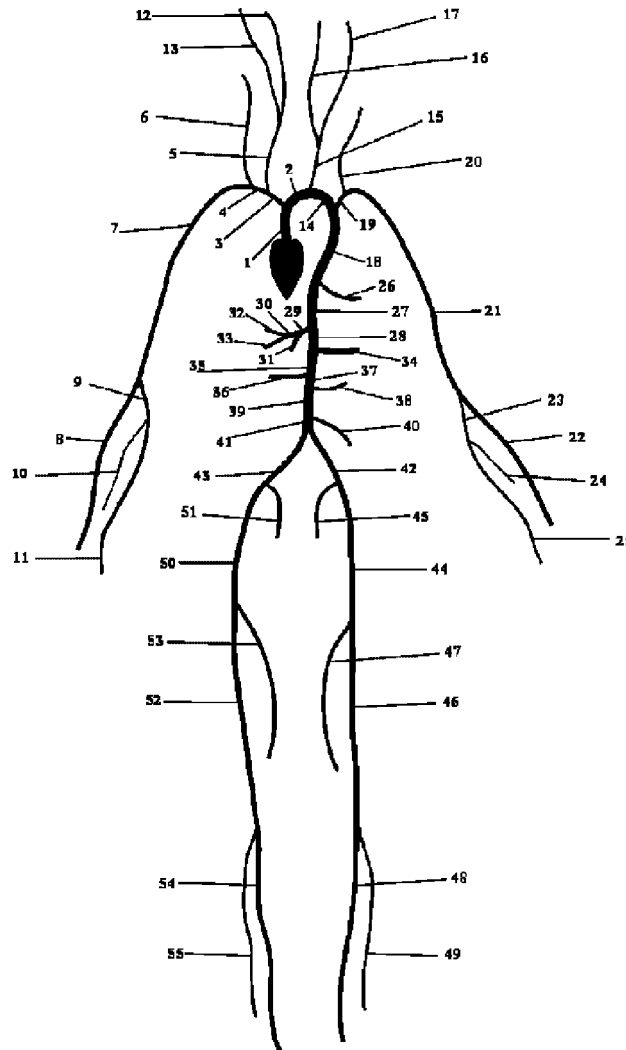
Figure 11. Connectivity of the 55 main arteries in the human arterial system.

form at the ascending aorta (artery 1), which has the form

$$A(t) = 1 - 0.597\delta(t)H[\delta(t)]; \quad \delta(t) = \sin(wt + 0.628) - 0.588$$

where $w = 2\pi/T$, $T = 1$ and $H(\delta)$ denotes the Heaviside step function. The graph of W_1 against time in Figure 12(b) represents the form of the input wave. For all computations a timestep $\Delta t = 10^{-5}$ and polynomial order $P = 9$ were used. The outflow condition when modelled with terminal resistance is calculated as described in Section 6.4.

Figures 12, 13 and 14 show eight time history graphs over a single cycle for three different arteries in the network: ascending aorta (artery 1), femoral artery (artery 46) and anterior

Table I. Data used in the computational model of the 55 arteries. This table combines the physiological data published in References [22, 20, 21].

#	Artery	Length (cm)	Area (cm^2)	β(kg s^{-2} cm^{-2})	R_t
1	Ascending Aorta	4.0	5.983	97	—
2	Aortic Arch I	2.0	5.147	87	—
3	Brachiocephalic	3.4	1.219	233	—
4	R. Subclavian I	3.4	0.562	423	—
5	R. Carotid	17.7	0.432	516	—
6	R. Vertebral	14.8	0.123	2590	0.906
7	R. Subclavian II	42.2	0.510	466	—
8	R. Radial	23.5	0.106	2866	0.82
9	R. Ulnar I	6.7	0.145	2246	—
10	R. Interosseous	7.9	0.031	12894	0.956
11	R. Ulnar II	17.1	0.133	2446	0.893
12	R. Internal Carotid	17.6	0.121	2644	0.784
13	R. External Carotid	17.7	0.121	2467	0.79
14	Aortic Arch II	3.9	3.142	130	—
15	L. Carotid	20.8	0.430	519	—
16	L. Internal Carotid	17.6	0.121	2644	0.784
17	L. External Carotid	17.7	0.121	2467	0.791
18	Thoracic Aorta I	5.2	3.142	124	—
19	L. Subclavian I	3.4	0.562	416	—
20	Vertebral	14.8	0.123	2590	0.906
21	L. Subclavian II	42.2	0.510	466	—
22	L. Radial	23.5	0.106	2866	0.821
23	L. Ulnar I	6.7	0.145	2246	—
24	L. Interosseous	7.9	0.031	12894	0.956
25	L. Ulnar II	17.1	0.133	2446	0.893
26	Intercostals	8.0	0.196	885	0.627
27	Thoracic Aorta II	10.4	3.017	117	—
28	Abdominal I	5.3	1.911	167	—
29	Celiac I	2.0	0.478	475	—
30	Celiac II	1.0	0.126	1805	—
31	Hepatic	6.6	0.152	1142	0.925
32	Gastric	7.1	0.102	1567	0.921
33	Splenic	6.3	0.238	806	0.93
34	Superior Mesenteric	5.9	0.430	569	0.934
35	Abdominal II	1.0	1.247	227	—
36	L. Renal	3.2	0.332	566	0.861
37	Abdominal III	1.0	1.021	278	—
38	R. Renal	3.2	0.159	1181	0.861
39	Abdominal IV	10.6	0.697	381	—
40	Inferior Mesenteric	5.0	0.080	1895	0.918
41	Abdominal V	1.0	0.578	399	—
42	R. Common Iliac	5.9	0.328	649	—
43	L. Common Iliac	5.8	0.328	649	—
44	L. External iliac	14.4	0.252	1493	—
45	L. Internal Iliac	5.0	0.181	3134	0.925
46	L. Femoral	44.3	0.139	2559	—
47	L. Deep Femoral	12.6	0.126	2652	0.885
48	L. Posterior Tibial	32.1	0.110	5808	0.724
49	L. Anterior Tibial	34.3	0.060	9243	0.716

Table I. *Continued.*

#	Artery	Length (cm)	Area (cm²)	β (kg s⁻² cm⁻²)	R_t
50	R. External Iliac	14.5	0.252	1493	—
51	R. Internal Iliac	5.1	0.181	3134	0.925
52	R. Femoral	44.4	0.139	2559	—
53	R. Deep Femoral	12.7	0.126	2652	0.888
54	L. Posterior Tibial	32.2	0.110	5808	0.724
55	R. Anterior Tibial	34.4	0.060	9243	0.716
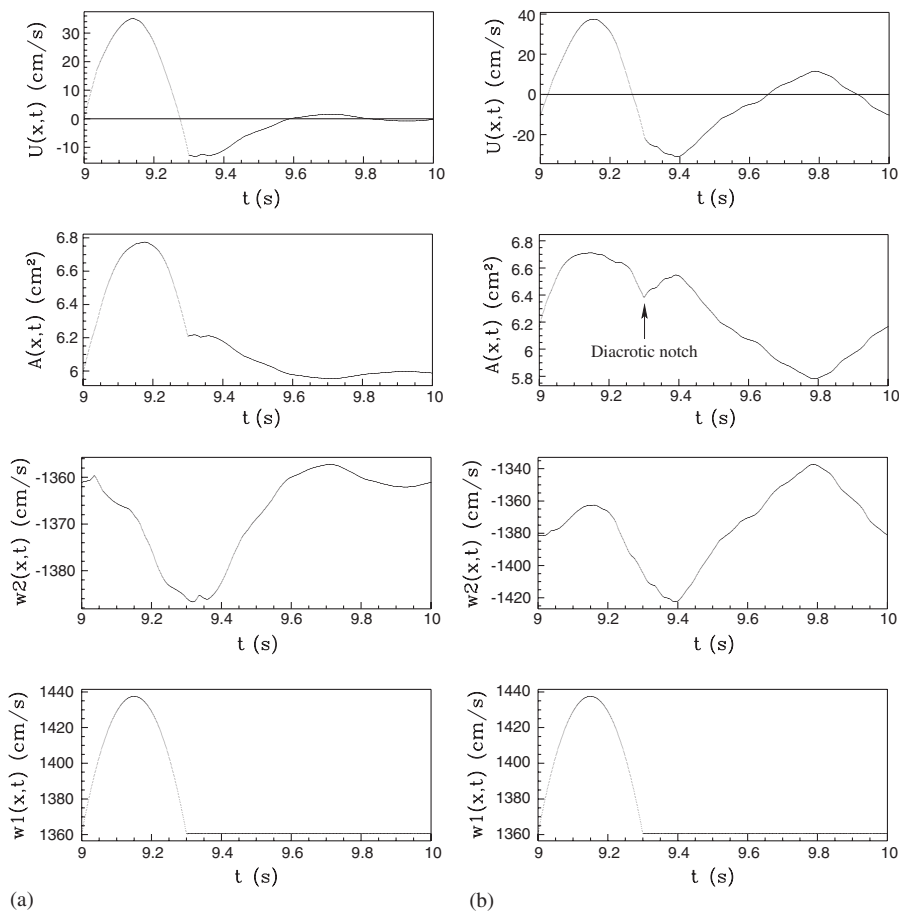
Figure 12. Time histories at the ascending aorta (artery 1) considering: (a) no terminal resistance and (b) terminal resistance. Plots of velocity, area and the characteristic variables W_2 and W_1.
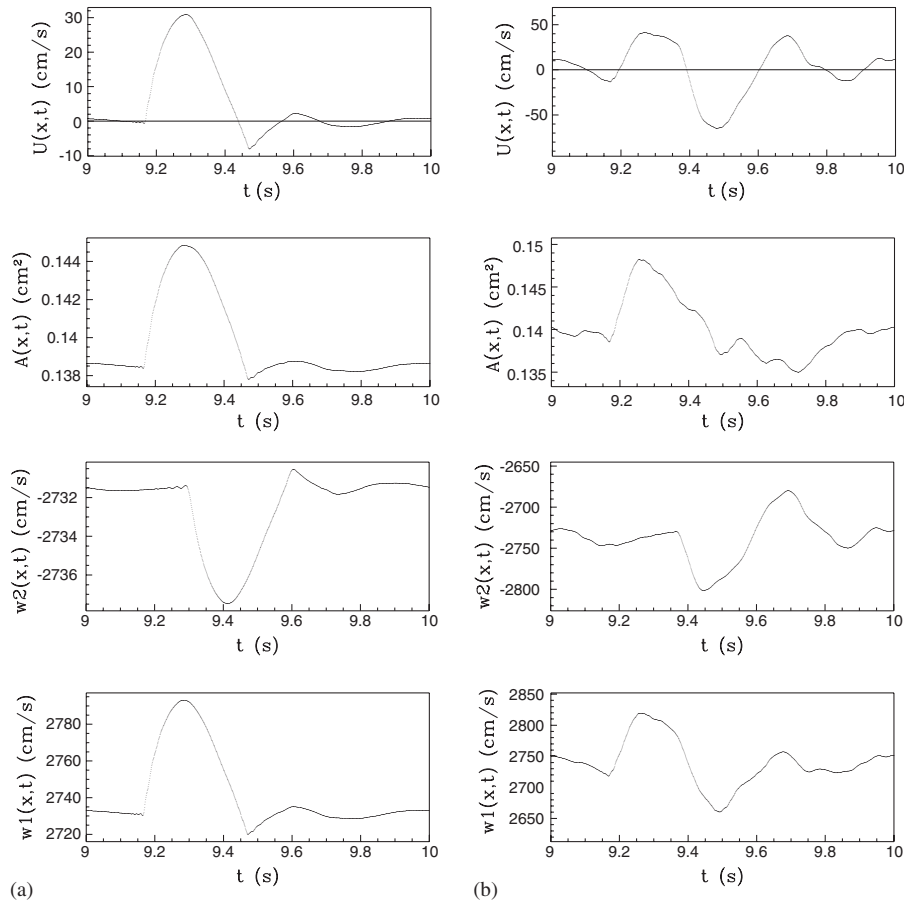
Figure 13. Time histories at the femoral artery (artery 46) considering: (a) no terminal resistance and (b) terminal resistance. Plots of velocity, area and the characteristic variables W_2 and W_1.

tibial (artery 49). The history point was at the start of each artery. The results are shown for a free outflow (i.e. no terminal resistance) and with terminal resistance applied.

For perfectly matched arteries there should be no backward travelling wave, W_2, if there is no terminal resistance (Figures 12(a), 13(a) and 14(a)), because there should be no reflections at the bifurcations and there are no reflections at the terminal vessels. Figure 14(a) shows that there is no W_2 wave at the anterior tibial artery. There is a small W_2 wave in some of the arteries, because they are not perfectly well-matched forward waves and consequently small reflections occur at the bifurcations.

The inclusion of resistance to the terminal arteries increases the number of waves in the system due to forward travelling waves being reflected at the terminal vessels and introduces backward travelling waves, W_2, which are re-reflected at the bifurcations, hence a complex pattern of waves occurs in the network. Since the reflection coefficients are close to 1 in the terminal vessels W_2 is similar in magnitude to W_1 and will have a large effect on the wave
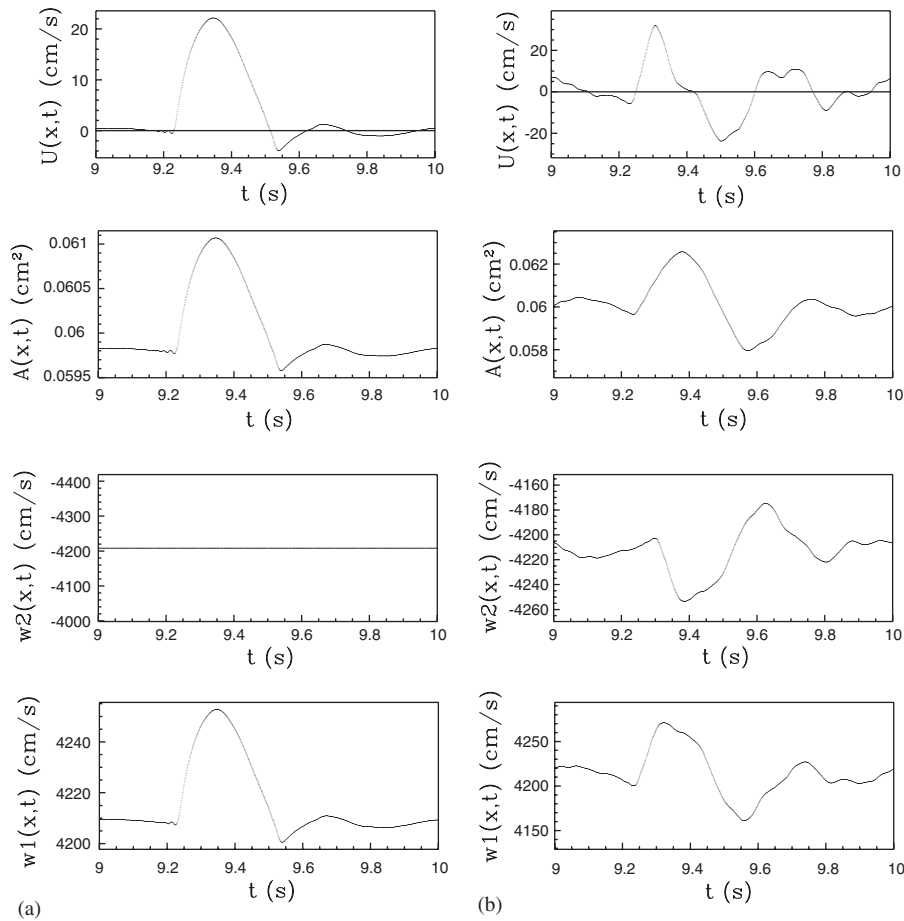
Figure 14. Anterior tibial artery (terminal artery 49). Time history comparison of waves forms with: (a) no terminal resistance and (b) terminal resistance. Plots of velocity, area and the characteristic variables W_2 and W_1.

forms, particularly in the end vessels, Figure 14(b). Introducing resistance has greatly changed the shapes of all the waves throughout the arterial network. The shape of the waves varies significantly from vessel to vessel whereas the shapes of the waves in the network with no terminal resistance were all very similar.

The inclusion of terminal resistance leads to more realistic results. Even though quantitative comparisons are difficult due to the lack of accurate values of the elastic properties of the arteries, the computed pressure (or area) waveforms show an increase in their peak value as we move down the system whilst the mean pressure slowly decreases. This behaviour is qualitatively similar to that observed in the human arterial system, see for instance the *in vivo* measurements by Mills *et al.* (1970) reproduced in Reference [23]. Terminal resistance also creates regions of flow reversal due to the reflected velocity wave and increases in area as a result of the re-enforcing effect of the reflected pressure wave. It has also produced a waveform
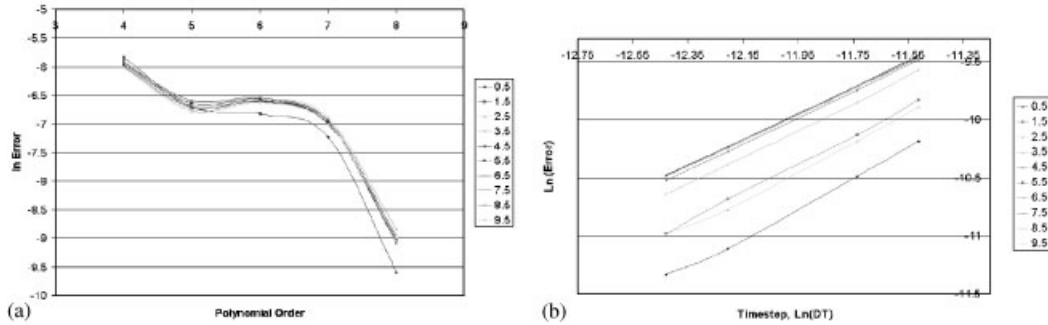
Figure 15. Logarithmic plot of velocity error at a point in the abdominal aorta (artery 39) against:
(a) polynomial order and (b) timestep.

which includes a diacrotic notch in the ascending aorta (artery 1). This is highlighted in the time evolution of the area depicted in Figure 12(b). This is also in agreement with *in vivo* data [23].

7.2. Convergence

Tests were done to show that increasing the polynomial order and decreasing the timestep the solution converged. Figure 15 displays the convergence curves of the error of the velocity in the abdominal aorta (artery 39) against the polynomial order (Figure 15(a)) and the timestep (Figure 15(b)) using the solution with $P = 9$ and $\Delta t = 10^{-5}$ as the reference solution for comparison. The error of the velocity was plotted every cycle for 10 cycles. Our results are presented for cycle 10.

8. CONCLUSIONS

Starting from the governing equations of the one-dimensional equations for blood flow in a tube of variable material properties we have formulated two numerical discretisations using Taylor–Galerkin and discontinuous Galerkin techniques. We have addressed the problem of applying appropriate boundary conditions at the terminal ends of a compliant artery or system of arteries using the characteristic equations for this hyperbolic system. Both schemes were applied to a model test case of an idealised stent inclusion in a tube to validate both approaches and to study the effect of the increased stiffness of the stent on the wave propagation pattern along the artery. The discontinuous Galerkin scheme was also tested on a tapered tube where physically reasonable results were obtained. Current work is focused on the development of discontinuous material properties.

Finally we considered the simulation of wave propagation in the human arterial system. The one-dimensional model of the compliant tube was adapted for a network of arteries by imposing suitable interface conditions at the bifurcation points where several branches meet. Waves are reflected at the bifurcations and these reflections lead to superimposition of waves which might result in increased peak pressures at other points of the arterial tree. To model these effects we have adopted a simplified model consisting of the 55 main arteries. The

missing arteries were simulated through a simple model of terminal resistance. The effect of the terminal resistance was investigated by comparing the wave patterns obtained with and without terminal resistance. The most important findings are that the terminal resistance generates regions of reversed flow and also produces a waveform in the ascending aorta which includes a diacrotic notch. The diacrotic notch is a physiological feature that has been observed in flow measurements *in vivo*.

ACKNOWLEDGEMENTS

REFERENCES

 1. Botnar R, Rappitsch G, Scheidegger MB, Liepsch D, Perktold K, Boesiger P. Hemodynamics in the carotid artery bifurcation: A comparison between numerical simulations and *in vitro* measurements. *Journal of Biomechanics* 2000; **33**:137–144.
 2. Hughes TH, Taylor C, Zarins C. Finite element modelling of blood flow in arteries. *Computer Methods in Applied Mechanics and Engineering* 1998; **158**:155–196.
 3. Quarteroni A, Tuveri M, Veneziani A. Computational vascular fluid dynamics: Problems, models and methods. *Computing and Visualisation in Science* 2000; **2**:163–197.
 4. Sherwin SJ, Shah O, Doorly DJ, Peiró J, Papaharilaou Y, Watkins N, Caro CG, Dumoulin CL. The influence of Out-of-plane geometry on the flow within a distal end-to-side anastomosis. *ASME Journal of Biomechanics* 2000; **122**:1–10.
 5. Formaggia L, Nobile F, Quarteroni A, Veneziani A. Multi-scale modelling of the circulatory system: a preliminary analysis. *Computing and Visualization in Science* 1999; **2**:75–83.
 6. Formaggia L, Nobile F, Quarteroni A. A one dimensional model for blood flow: application to vascular prosthesis. In Babuska I, Miyoshi T, Ciarlet PG (eds). *Mathematical Modeling and Numerical Simulation in Continuum Mechanics*, Lecture Notes in Computational Science and Engineering, vol. 19. Berlin: Springer-Verlag, 2002; 137–153.
 7. Brook BS, Falle SAEG, Pedley TJ. Numerical solution for unsteady gravity-driven flows in collapsible tubes: evolution and roll-wave instability of a steady state. *Journal of Fluid Mechanics* 1999; **396**:223–256.
 8. Hunter PJ. Numerical solution of arterial blood flow. *Master's Thesis*, University of Auckland, 1972.
 9. Womersley JR. Method for the calculation of velocity, rate of flow and viscous drag in arteries when the pressure gradient is known. *Journal of Physiology* 1955; **127**:553–563.
10. Tsangaris S, Drikakis D. Pulsating blood flow in an initially stressed, anisotropic elastic tube: linear approximation of pressure waves. *Medical and Biological Engineering and Computation* 1989; **27**:82–88.
11. Canic S, Kim EH. Mathematical analysis of the quasilinear effects in a hyperbolic model of blood flow through compliant axi-symmetric vessels. *Mathematical Methods in the Applied Sciences* 2003; **26**:1–26.
12. Formaggia L, Gerbeau J-F, Nobile F, Quarteroni A. On the coupling of 3D and 1D Navier-Stokes equations for flow problems in compliant vessels. *Computer Methods in Applied Mechanics and Engineering* 2001; **191**: 561–582.
13. Thompson KW. Time dependent boundary conditions for hyperbolic systems. *Journal of Computational Physics* 1987; **68**:1–24.
14. Hedstrom GW. Nonreflecting boundary conditions for nonlinear hyperbolic systems. *Journal of Computational Physics* 1979; **30**:222–237.
15. Godlewski E, Raviart P-A. *Numerical Approximation of Hyperbolic Systems of Conservation Laws*, Applied Mathematical Sciences, vol. 118. New York: Springer, 1996.
16. Sherwin SJ. Dispersion analysis of the continuous and discontinuous Galerkin formulations. In Cockburn B, Karniadakis GE, Shu CW (eds). *Discontinuous Galerkin Methods: Theory, Computation and Application*, 2000; 425–431.

17. Cockburn B, Shu CW. TVB Runge-Kutta projection discontinuous Galerkin finite element methods for conservation laws II: general framework. *Math. Comm.* 1989; **52**:411–435.
18. Lomtev I, Quillen CW, Karniadakis G. Spectral/hp methods for viscous compressible flows on unstructured 2d meshes. *Journal of Computational Physics* 1998; **144**:325–357.
19. Lighthill J. *Waves in Fluids*. Cambridge: Cambridge University Press, 1978.
20. Stergiopulos N, Young DF. Computer simulation of arterial flow with applications to arterial and aortic stenoses. *Journal of Biomechanics* 1992; **25**(12):1477–1488.
21. Wang JJ, Parker KH. Wave propagation in a model of the arterial circulation. *Journal of Biomechanics* 2003, at press.
22. Westerhof N, Bosman F, De Vries CJ, Noordergraaf A. Analog studies of the human systemic arterial tree. *Journal of Biomechanics* 1969; **2**:121–143.
23. Nichols WW, O'Rourke MF. *McDonald's Blood Flow in Arteries*. Edward Arnold (3rd ed.). 1990.